# Comparability of [18F]THK5317 and [11C]PIB blood flow proxy images with [18F]FDG PET in Alzheimer's disease

Elena Rodriguez-Vieitez[1], Antoine Leuzy[1], Konstantinos Chiotis[1], Laure Saint-Aubert[1], Anders Wall[2], and Agneta Nordberg[1,3]

[1]Department NVS, Centre for Alzheimer Research, Translational Alzheimer Neurobiology, Karolinska Institutet, Stockholm, Sweden

[2]Section of Nuclear Medicine and PET, Department of Surgical Sciences, Uppsala University, Uppsala, Sweden

[3]Department of Geriatric Medicine, Karolinska University Hospital Huddinge, Stockholm, Sweden

Published: 22 April 2016

by Sage Journals for the International Society for Cerebral Blood Flow and Metabolism

in the Journal of Cerebral Blood Flow and Metabolism

doi: 10.1177/0271678X16645593

pii: 0271678X16645593

# Comparability of [$^{18}$F]THK5317 and [$^{11}$C]PIB blood flow proxy images with [$^{18}$F]FDG PET in Alzheimer's disease

Elena Rodriguez-Vieitez[1,†], Antoine Leuzy[1,†], Konstantinos Chiotis[1], Laure Saint-Aubert[1], Anders Wall[2], and Agneta Nordberg[1,3,*]

[1]Department NVS, Centre for Alzheimer Research, Translational Alzheimer Neurobiology, Karolinska Institutet, Stockholm, Sweden
[2]Section of Nuclear Medicine and PET, Department of Surgical Sciences, Uppsala University, Uppsala, Sweden
[3]Department of Geriatric Medicine, Karolinska University Hospital Huddinge, Stockholm, Sweden
[†]These authors contributed equally to these work

**Running title:** Blood flow proxy images in Alzheimer's disease

[*]**Correspondence to:** Agneta Nordberg, MD, PhD
Division of Translational Alzheimer Neurobiology
Karolinska University Hospital Huddinge
Novum 5th Floor, Blickagången 6
S-141 57 Stockholm, Sweden 141 57
E-mail: agneta.k.nordberg@ki.se
Tel.: +46 8 585 85467; Fax: +46 8 585 85470

**Funding:** This work was financially supported by grants from the Swedish Research Council (project 05817), the Swedish Foundation for Strategic Research (SSF), the Karolinska Institutet Strategic Neuroscience program, the Stockholm County Council-Karolinska Institutet regional agreement on medical training and clinical research (ALF grant), Swedish Brain Power, the Swedish Brain Foundation, the Alzheimer Foundation in Sweden, the Dementia Association, the EU FP7 large-scale integrating project INMiND (http://www.uni-muenster.de/INMiND), the Foundation for Old Servants, Karolinska Institutet's Foundation for Aging Research, Gun and Bertil Stohne's Foundation, Loo and Hans Osterman's Foundation, the Åhlén Foundation, and the Wenner-Gren Foundation.

**Data availability:** Data can be accessed after contact with the authors and upon written agreement.

## Abstract

For amyloid PET tracers, the simplified reference tissue model (SRTM) derived ratio of influx rate in target relative to reference region ($R_1$) has been shown to serve as a marker of brain perfusion, and, due the strong coupling between perfusion and metabolism, as a proxy for glucose metabolism. In the present study, eleven prodromal Alzheimer's disease (AD) and nine AD dementia patients underwent [$^{18}$F]THK5317 and [$^{18}$F]FDG PET in order to assess the possible use of early-phase [$^{18}$F]THK5317 and $R_1$ as proxies for brain perfusion, and thus, of glucose metabolism. Discriminative performance (prodromal vs dementia AD) of [$^{18}$F]THK5317 early-phase SUVr and $R_1$) was compared to that of [$^{11}$C]PIB and [$^{18}$F]FDG. Strong positive correlations were found between [$^{18}$F]THK5317 (early-phase, $R_1$) and [$^{18}$F]FDG, particularly in frontal and temporoparietal regions. Differences in correlations between early-phase and $R_1$ ([$^{18}$F]THK5317 and [$^{11}$C]PIB) and [$^{18}$F]FDG, were not statistically significant, nor were differences in area under the curve values in the discriminative analysis. Our findings suggest that early-phase [$^{18}$F]THK5317 and $R_1$ provide information on brain perfusion, closely related to glucose metabolism. As such, a single PET study with [$^{18}$F]THK5317 may provide information about both tau pathology and brain perfusion in AD, with potential clinical applications.

**Keywords:** Alzheimer's disease; early-phase [$^{11}$C]PIB; early-phase [$^{18}$F]THK5317 PET; [$^{18}$F]FDG; SRTM $R_1$

## Introduction

Increasing evidence from *in vivo* and *in vitro* studies suggests that Alzheimer's disease (AD) begins with the deposition of amyloid-β (Aβ), leading to downstream neurodegenerative changes, including tau hyperphosphorylation. Widely applied to imaging fibrillary Aβ, the success of amyloid positron emission tomography (PET) with carbon-11 Pittsburgh Compound-B ([$^{11}$C]PIB) and fluorinated alternatives such as [$^{18}$F]florbetapir and [$^{18}$F]flutemetamol have led to worldwide efforts aimed at the development of selective tau PET tracers [1]. These efforts have resulted in several promising candidate compounds now in clinical studies, including the second-generation quinolone derivative [$^{18}$F]THK5317, previously known as *(S)*-[$^{18}$F]THK5117 [2].

In addition to providing a measure of Aβ plaque pathology, there is evidence to suggest that the early-phase of dynamic [$^{11}$C]PIB PET can capture additional information closely related to cerebral glucose metabolism, comparable to that obtained using 2-deoxy-2-[$^{18}$F]fluoro-D-glucose ([$^{18}$F]FDG) PET [3-8]. By using the unidirectional influx constant ($K_1$) and early time-frame [$^{11}$C]PIB uptake values—measures shown to correlate with cerebral blood flow (CBF)—regional metabolism was estimated due the strong coupling between perfusion and glucose metabolism [9]. Further, using both [$^{11}$C]PIB and [$^{18}$F]florbetapir, dynamic PET data fitted using the simplified reference tissue model (SRTM) [10] to obtain $R_1$—the ratio of $K_1$ in target and reference tissue—has been found to serve as a reliable measure of relative brain perfusion [6,11]. Approaches incorporating these measurements may decrease the need for dual-tracer (e.g. [$^{11}$C]PIB and [$^{18}$F]FDG) PET studies, resulting in decreased costs, patient discomfort, and radiation exposure. To date, however, no studies have examined whether the early-phase of [$^{18}$F]THK5317 or $R_1$ can provide perfusion information, and thus, a measure comparable to regional cerebral glucose metabolism.

The overarching aim of the present study was to thus explore the possible use of [$^{18}$F]THK5317 early-phase standardized uptake value ratios (SUVr) and SRTM $R_1$ as proxies for brain perfusion in AD, and to compare these measures with glucose metabolism as measured

using [$^{18}$F]FDG PET. To this end, we compared early-phase [$^{18}$F]THK5317 SUVr images and $R_1$ estimates with [$^{18}$F]FDG SUVr, both within regions of interest (ROIs), and at the voxel level. In addition, with dual PET imaging of tau and amyloid being an increasingly likely prospect in the years to come, we compared [$^{18}$F]THK5317 and [$^{11}$C]PIB (early-phase SUVr and $R_1$) with respect to their correlational strength to [$^{18}$F]FDG SUVr. The classification accuracy of these parameters, in terms of their ability to discriminate between prodromal and AD dementia patient groups, was likewise investigated.

## Materials and Methods

### Study Population

Data from eleven mild cognitive impairment (MCI), and nine AD patients were used in the present investigation. All were recruited at the Department of Geriatric Medicine, Karolinska University Hospital Huddinge, Stockholm, Sweden, as part of another multitracer PET study [12]. All patients underwent a comprehensive routine assessment procedure, including a physical examination, evaluation of neurological and psychiatric status, apolipoprotein E (ApoE) genotyping from blood sample, serum and urine analysis, structural magnetic resonance imaging (MRI), cerebrospinal fluid sampling, and neuropsychological assessment.

Patients with AD fulfilled the NINCDS-ADRDA criteria for probable AD [13], and MCI was diagnosed according to the Petersen criteria [14,15]. In all cases, diagnosis was reached via a consensus based committee approach, which included neurologists, clinical neuropsychologists, and specialist nurses. MCI patients were considered as prodromal AD on the basis of episodic memory loss and positive [$^{11}$C]PIB PET findings [16].

All patients provided written informed consent to participate in the present study, which was conducted according to the declaration of Helsinki and subsequent revisions. Ethical approval was obtained from the regional human ethics committee of Stockholm and the Faculty of Medicine and Radiation Hazard Ethics Committee of Uppsala University Hospital, Uppsala, Sweden.

**Image Acquisition**

[$^{18}$F]THK5317 and [$^{11}$C]PIB PET scans were performed at the Uppsala PET Centre, Uppsala, Sweden, on an ECAT EXACT HR+ (Siemens/CTI, Knoxville, TN) or a Discovery ST PET/CT scanner (GE Medical Systems, Milwaukee, WI). The orbitomeatal line was used to center the head of the participants, with PET data acquired in 3D mode, yielding a 155 mm field of view. Both tracers were synthesized according to standard good manufacturing processes, as previously described [17,18], with [$^{18}$F]THK5317 selected over the racemic mixture due to reports of lower non-specific binding and faster kinetics with the (*S)*-enantiomeric form (Victor Villemagne, unpublished data), similar to that shown for two other tau tracers of the same family [19,20].

The dynamic [$^{18}$F]THK5317 PET acquisition consisted of 22 frames acquired over 60 min (6 x 10s, 3 x 20s, 2 x 30s, 2 x 60s, 2 x 150s, 4 x 300s, and 3 x 600s frames) after intravenous injection of 211 ± 41 MBq. The dynamic [$^{11}$C]PIB PET acquisition consisted of 24 frames acquired over 60 min (4 × 30s, 9 × 60s, 3 × 180s and 8 × 300s) after intravenous injection of 253 ± 69 MBq. Images were reconstructed using normalization- and attenuation-weighted ordered subset expectation maximization (NAW-OSEM; 6 iterations, 8 subsets) applying all appropriate corrections and a 4 mm Hanning post-filter.

[$^{18}$F]FDG PET studies were performed as part of routine clinical practice at the Department of Nuclear Medicine, Karolinska University Hospital Huddinge, Stockholm, Sweden, using a Biograph mCT PET/CT scanner (Siemens/CTI, Knoxville, TN). The imaging protocol consisted of a 15 min static acquisition performed 30 min after an intravenous bolus injection of 3MBq/kg. All patients underwent a T1-weighted MRI scan, which was used for segmentation and ROI definition.

**Image Processing**

The dynamic PET data for [$^{18}$F]THK5317 and [$^{11}$C]PIB was realigned to correct for inter-frame patient movement using the software VOIager (v.4.0.7, GE Healthcare, Uppsala, Sweden). Individual dynamic [$^{18}$F]THK5317 and [$^{11}$C]PIB PET scans were co-registered onto the

individual T1-weighted MRI using PMOD image registration and fusion tool (PFUS) (v.3.5, PMOD Technologies Ltd., Adliswil, Switzerland). The MRI of each patient was classified into grey matter (GM), white matter (WM) and cerebrospinal fluid (CSF) using the unified segmentation algorithm of SPM. An inclusive binary GM mask was then created by applying a threshold of 0.3 to the resultant probabilistic GM maps (0, no tissue; 1, tissue with >30% probability of belonging to GM).

As part of the segmentation algorithm an inverse nonlinear transform parameter file was generated, enabling transformation of data from Montreal Neurological Institute (MNI) space back into each individual's native T1 image space. This was used to spatially warp a probabilistic atlas [21]—comprising 49 regions—back into native T1 space for each subject. These atlases were then multiplied by their corresponding GM masks, yielding subject specific GM ROIs. Subsequently, ROIs were grouped—using a weighted average approach incorporating the number of voxels per volume—into frontal (superior, middle, inferior frontal gyri), medial temporal (hippocampus, parahippocampus, lingual and fusiform gyri), lateral temporal (superior, middle, inferior temporal gyri), posterior cingulate, parietal (upper and lower lateral remainders), occipital (lateral remainder, cuneus), and global cortical composite regions.

## PET Quantification

Using individual GM atlases, regional time-activity curves (TACs) were extracted from dynamic [$^{18}$F]THK5317 and [$^{11}$C]PIB PET data by applying the PMOD Kinetic Modeling Tool (PKIN). [$^{18}$F]THK5317 $R_1$ and [$^{11}$C]PIB $R_1$ were calculated using SRTM [10], with cerebellar GM as reference region, using PMOD. Voxelwise $R_1$ maps were also created using the PMOD Pixelwise Modeling Tool (PXMOD). [$^{11}$C]PIB and [$^{18}$F]FDG SUVr maps were calculated by normalizing 40-60 min [$^{11}$C]PIB and 30-45 min [$^{18}$F]FDG summation images to mean cerebellar GM activity, respectively, using SPM8. Individualized ROIs from the preceding atlas-creation step were then applied to SUVr maps to extract regional values. All patients were classified as [$^{11}$C]PIB positive using the composite neocortical SUVr and a cutoff of > 1.41 derived from

a previously characterized population of normally distributed healthy controls [22].

### Selection of [$^{18}$F]THK5317 and [$^{11}$C]PIB early-phase intervals

Data from the early-phase of [$^{18}$F]THK5317 were generated by frame time-weighted summation, using a range of initial time points ($T_0$ = 0, 1, and 2 min) and frame durations (1-10 min). Early-phase SUVr values were subsequently calculated for each time period by normalizing to activity within the cerebellar cortex over the corresponding interval. Using nine randomly selected patients (four prodromal AD and five AD), intra-subject correlations (Pearson's *r*) between early-phase [$^{18}$F]THK5317 and [$^{18}$F]FDG SUVr—as well as between early-phase [$^{18}$F]THK5317 SUVr and [$^{18}$F]THK5317 $R_1$—were calculated across all ROIs from the above described atlas. The optimum early-frame interval was then determined as that corresponding to the maximum average correlation coefficient between early-phase [$^{18}$F]THK5317 and $R_1$, among all intervals investigated [5]. Regional early-phase [$^{18}$F]THK5317 SUVr values were subsequently computed across all subjects using this optimized interval and selected for the remaining analyses. An optimal time window of 1-8 min was adopted for [$^{11}$C]PIB on the basis of previous findings showing high correlations between early-phase SUVr, $K_1$, and [$^{18}$F]FDG SUVr [5].

### Relationship between early-phase [$^{18}$F]THK5317, early-phase [$^{11}$C]PIB and [$^{18}$F]FDG SUVr

In order to test the assumption that $R_1$ and early-phase [$^{18}$F]THK5317 SUVr can provide indirect measures of regional glucose metabolism, ROI based and voxelwise correlation analyses between these parameters and [$^{18}$F]FDG SUVr were conducted. In a second step, early-phase [$^{18}$F]THK5317 and early-phase [$^{11}$C]PIB were correlated. To compare the potential of both [$^{18}$F]THK5317 and [$^{11}$C]PIB early-phase measures to serve as proxies of glucose metabolism, both were compared to [$^{18}$F]FDG SUVr at regional and voxel levels, using Pearson *r*.

## Voxelwise Analyses Methods

Voxelwise $R_1$, early-phase SUVr, and [$^{18}$F]FDG SUVr maps were used to perform voxelwise correlations, both uncorrected and corrected for multiple comparisons, using the Biological Parametric Mapping software package (BPM; Matlab, v.3.3) [23] in two-by-two comparisons. All PET images were first registered onto the MNI space, smoothed by an 8-mm FWHM Gaussian filter, and masked using an apriori GM mask. BPM correlation maps were thresholded at $p < 0.001$ (uncorrected, with cluster extent $k \geq 20$ voxels), and then corrected for multiple comparisons using a family-wise error (FWE) rate Bonferroni correction ($p < 0.05$). Resulting correlation maps (uncorrected and FWE corrected) were projected onto a group average surface using the cortical parcellation of FreeSurfer, v.5.3 (https://surfer.nmr.mgh.harvard.edu/).

## Statistical Analysis

All statistical analyses were performed in R (v.3.1.2, The R Foundation for Statistical Computing, Vienna, Austria), with an uncorrected $p$ value of $< 0.05$ used to indicate statistical significance. Patient characteristics were compared using Mann Whitney U and chi-square tests. Pearson's product moment correlation analyses between outcome measures were conducted on a region-by-region basis across all subjects. All ROI based correlations were corrected for multiple-comparison using the Bonferroni method. In order to compare the discriminative power of [$^{18}$F]THK5317/ [$^{11}$C]PIB $R_1$, early-phase [$^{18}$F]THK5317/ [$^{11}$C]PIB SUVr, and [$^{18}$F]FDG—with respect to the separation of prodromal and AD dementia groups—receiver operating characteristic (ROC) analyses were performed with ROI based values in order to generate area under the curve (AUC) values for each ROI. Bootstrapping with 2000 resampling iterations was then used to compare AUC calculations on a two-by-two basis, using the R package *pROC* (v.1.8) [24]. In order to test whether the difference between correlations for [$^{18}$F]THK5317/ [$^{11}$C]PIB $R_1$ and early-phase [$^{18}$F]THK5317/ [$^{11}$C]PIB SUVr vs [$^{18}$F]FDG SUVr was significant, Williams' (1959) modification of Hotelling's t-test was performed, using the R package *cocor* (v.1.1-1) [25].

## Results

Demographic and clinical data for prodromal and AD dementia groups are displayed in Supplementary Table 1. No group differences were found with respect to age, sex, or percent carriage of the ApoE ε4 allele. MMSE scores were lower in the AD dementia group ($p < 0.05$). Figure 1 shows the results of within-subject correlation analyses in the test subset of nine patients, between early-phase [$^{18}$F]THK5317 SUVr and both [$^{18}$F]THK5317 $R_1$ and [$^{18}$F]FDG SUVr, across the various time intervals investigated. The period 0-3 min (frames 1-11) was found to be the interval where [$^{18}$F]THK5317 SUVr had the highest correlations (mean ± SD Pearson's *r* of test group) with both $R_1$ ($r = 0.995 \pm 0.002$) and [$^{18}$F]FDG ($r = 0.811 \pm 0.051$). Representative images for the optimum 0-3 min early-phase [$^{18}$F]THK5317, 1-8 min early-phase [$^{11}$C]PIB SUVr, [$^{18}$F]THK5317 $R_1$, [$^{11}$C]PIB $R_1$, and [$^{18}$F]FDG are shown in Figure 2.

After identification of this optimal early-phase interval, correlation analysis was repeated across all 20 subjects. Significant positive correlations were found for both [$^{18}$F]THK5317 $R_1$ vs [$^{18}$F]FDG SUVr, and for early (0-3 min) [$^{18}$F]THK5317 SUVr vs [$^{18}$F]FDG SUVr across all regions analyzed with the strongest correlations observed in the parietal, lateral temporal, and occipital cortices (Table 1). Representative regression plots are shown in Figure 3. Significant positive correlations between early-phase [$^{18}$F]THK5317 SUVr and $R_1$ neared 1 across all regions analyzed, with all regions retaining significance following multiple comparison correction. Strong correlations were observed between early-phase [$^{18}$F]THK5317 and early-phase [$^{11}$C]PIB SUVr across all ROIs.

Voxelwise correlation analysis showed widespread positive associations between early-phase [$^{18}$F]THK5317 SUVr vs [$^{18}$F]FDG within the dorsolateral prefrontal cortex, primary sensory-motor strips, parietal and temporal cortices, as well as the temporoparietal carrefour and frontotemporal oppercula (Figure 4A). Medially, correlations were observed in the parahippocampal and fusiform gyri, cuneus/precuneus, and paracentral lobule, as well as in the dorsomedial prefrontal cortex, and cingulate gyri. A similar pattern was observed for [$^{18}$F]THK5317 $R_1$ vs [$^{18}$F]FDG—though with greater involvement of the cuneus, inferior temporal gyri, and anterior cingulate (Figure 4C). Early-phase [$^{18}$F]THK5317 and

[$^{18}$F]THK5317 $R_1$ were found to correlate positively across most cortical regions (Figure 4E). Few findings—in terms of percentage of ROIs—however, survived FWE correction for multiple comparisons: 33% (early [$^{18}$F]THK5317 SUVr vs [$^{18}$F]FDG, Figure 4B**),** 20% ($R_1$ vs [$^{18}$F]FDG, Figure 4d), and 63% (early-phase [$^{18}$F]THK5317 vs [$^{18}$F]THK5317 $R_1$, Figure 4F). Surviving results were located primarily in frontal and temporoparietal regions. Cluster extents and within cluster maxima (uncorrected and FWE corrected) are reported in Supplementary Tables 2-4. No negative correlations were observed between outcome measures.

Discriminatory analysis (prodromal AD vs AD dementia) using ROC derived AUC values showed that the highest values for all PET parameters were generally seen in the parietal, lateral temporal, and posterior cingulate cortices (Table 2). No significant differences, however, were found between AUC values for [$^{18}$F]THK5317 (early-phase SUVr and $R_1$), [$^{11}$C]PIB (early-phase SUVr and $R_1$), and [$^{18}$F]FDG (Table 2). Correlation coefficients for early phase SUVr and $R_1$ ([$^{18}$F]THK5317 and [$^{11}$C]PIB) vs [$^{18}$F]FDG reached statistical significance across all cortical ROIs (Table 3). No significant differences were found when correlation coefficients were compared across ROIs.

## Discussion

The present study showed for the first time that [$^{18}$F]THK5317 blood flow indices (early-phase SUVr and $R_1$) correlate strongly with [$^{18}$F]FDG SUVr. These results held at both the regional and voxel level. Overall, no significant differences in the discriminatory ability of investigated parameters were found. Secondarily, head-to-head comparison between early-phase SUVr of [$^{18}$F]THK5317 and [$^{11}$C]PIB, in terms of correlational strength to [$^{18}$F]FDG, showed no differences.

Although the interval between time 0 and 3 min was chosen as the optimal early-phase for [$^{18}$F]THK5317 in the present study, given that it provided the greatest correlation with $R_1$, similarly high correlations were obtained when extending a minute on either side of the selected upper limit (0-2 or 0-4 min). Starting at the time of injection, however, ensured capture of the initial phase of tracer influx up to the time of peak concentration, $t_{max}$, which occurred within 2

to 3 min of tracer administration. On the basis of our findings, starting at 1 or 2 min post injection would likewise prove suitable; as such, the period used for the creation of the [$^{18}$F]THK5317 summation image could be determined locally as a function of preference.

Visual inspection of representative early-phase [$^{18}$F]THK5317, early-phase [$^{11}$C]PIB, [$^{18}$F]THK5317 $R_1$, [$^{11}$C]PIB $R_1$, and [$^{18}$F]FDG normalized uptake images shows clear-cut similarities in intensity patterns. While uptake within association cortices was greater in the patient with prodromal AD, in comparison to the patient with AD dementia, both patients showed similar perfusion and metabolism levels in subcortical structures, consistent with previous findings using [$^{18}$F]FDG and perfusion single photon emission tomography (SPECT) [26,27]. Interestingly, an asymmetrical pattern of temporo-parietal hypoperfusion in the AD patient coincides with a similarly asymmetrical hypometabolism in the same cortical regions, which can be appreciated visually.

The high ROI and voxel based correlations observed for [$^{18}$F]THK5317 (early-phase SUVr and $R_1$) vs [$^{18}$F]FDG indicates good coupling between blood flow and glucose metabolism in the brain at resting-state. The inter-subject correlation coefficients between early-phase SUVr and $R_1$ of [$^{18}$F]THK5317 were likewise very high, indicating that early-phase [$^{18}$F]THK5317 measures brain perfusion relative to the cerebellum. Similar findings were obtained for [$^{11}$C]PIB, with no significant differences observed following comparison of correlation coefficients with those obtained using [$^{18}$F]THK5317. Though application of multiple comparison correction reduced our voxelwise findings, retained significance despite a small sample size and the conservative nature of the FWE-rate approach support the assertion that that early-phase SUVr and $R_1$ of [$^{18}$F]THK5317 provide proxy measures of regional relative blood flow and thus, of brain metabolism.

Several studies have compared the discriminative ability of glucose metabolism and brain perfusion, as measured by [$^{18}$F]FDG SUVr, early-phase amyloid PET, $^{99m}$Tc-HMPAO SPECT, and arterial spin labeling (ASL) MRI, with respect to the differentiation of AD from healthy controls [5,28,29]. These studies have shown the parietal, temporal, and posterior cingulate cortices to possess the best discriminative performance. Few studies, however, have specifically

compared glucose metabolism and brain perfusion with respect to the separation of patients in the prodromal and dementia stages of AD. In the present study, AUC values were highest in these regions, across all parameters. Though AUC values for the discrimination between prodromal and dementia stages of AD were higher for perfusion markers compared to [$^{18}$F]FDG in the frontal cortex—a finding that raised the tempting interpretation of relatively preserved brain perfusion in prodromal AD patients suggesting compensatory mechanisms at early stages of AD, as previously reported [30]—no statistically significant differences were found between AUC values obtained from perfusion compared to [$^{18}$F]FDG measures within the frontal region, nor across the remaining ROIs.

The cerebellar cortex was selected as the reference region for [$^{18}$F]THK5317 and [$^{11}$C]PIB estimates due to previous reports of it lacking NFTs and Congo red/ thioflavin-S positivity, respectively [31,32]. Though consensus has yet to be reached as to which reference region is most suitable for normalization of [$^{18}$F]FDG SUV images, the pons has frequently been selected due to it being purported to be the brain region that is least affected, from a metabolic standpoint, in AD [33]. The cerebellar cortex was used in the present study, however, to achieve consistency with respect to the reference region used for [$^{18}$F]THK5317 and [$^{11}$C]PIB; in this respect, the metabolism of the cerebellar cortex has been shown to be well preserved in mild-to-moderate AD [34], and has likewise been shown to be a good reference region for brain perfusion [35,36].

Certain methodological aspects, however, limit interpretation of the present findings. In addition to the relatively limited sample size, we did not have any cognitively normal controls or patients with non-AD tauopathies, groups desirable to include in order to cover a wider range of outcome measures. Further, [$^{18}$F]FDG SUVr is a semi-quantitative measure of glucose metabolism. However, it has been previously validated against fully quantitative measures of cerebral glucose metabolic rate [34], and has been widely used in previous investigations examining the use of early-phase of [$^{11}$C]PIB and [$^{18}$F]florbetapir as proxies of brain perfusion [5,6,7,11]. More accurate absolute measurements of brain perfusion using ASL MRI or $^{15}$O-water PET—measures that have been shown to correlate well with [$^{18}$F]FDG [37,38] or surrogate

measures of absolute brain perfusion such as those obtained by washout allometric reference method as demonstrated for [$^{11}$C]PIB PET [49,40]—would potentially also have allowed for more accurate comparison with $R_1$, itself a relative measure only.

Despite these caveats, our findings suggest that early-phase SUVr and SRTM derived $R_1$ of [$^{18}$F]THK5317 provide information on CBF, being closely correlated to glucose metabolism. The comparable discriminatory power observed across measures, in addition to the lack of statistical differences between associational strength to [$^{18}$F]FDG, suggests that early-phase SUVr/$R_1$ of [$^{18}$F]THK5317 and [$^{11}$C]PIB may both prove substitutes for [$^{18}$F]FDG. An interesting possibility given the high cost of [$^{18}$F]FDG investigations, [41] tracer selection could be based on feasibility, desired objectives, and availability of dynamic scanning protocols ($R_1$). Further prospective studies, including those incorporating additional tau and fluorine-18 Aβ PET imaging agents, are required to validate and extend these findings. Additional comparative clinical studies with [$^{18}$F]FDG will also be of value to establish the diagnostic utility of these measures in both AD and non-AD tauopathies.

## Acknowledgments

We would like to express our gratitude the patients who participated in the PET studies and their relatives. We also wish to thank the staff at the Uppsala PET Centre and Memory Clinic, Karolinska University Hospital Huddinge, as well Johan Lilja for support related to the imaging software VOIager (v.4.0.7, GE Healthcare, Uppsala, Sweden).

## Author contributions

ERV, AL, AW, and AN were responsible for the study design; AN coordinated the study. ERV, AL, KC, and LSA were responsible for image processing and analysis. AW coordinated the PET investigations. ERV and AL were responsible for drafting of the manuscript. All authors critically revised the final version of the manuscript.

## Disclosure/Conflict of Interest

The authors declare no conflict of interest.

Supplementary information is available at the Journal of Cerebral Blood Flow & Metabolism website – www.nature.com/jcbfm.

## References


1. Villemagne VL, Fodero-Tavoletti MT, Masters CL, Rowe CC. Tau imaging: early progress and future directions. *Lancet Neurol.* 2015; 14(1)**:** 114-24.

2. Okamura N, Furumoto S, Harada R, Tago T, Yoshikawa T, Fodero-Tavoletti M *et al.* Novel 18F-labeled arylquinoline derivatives for noninvasive imaging of tau pathology in Alzheimer disease. *J. Nucl. Med.* 2013; 54(8)**:** 1420-7.

3. Blomquist G, Engler H, Nordberg A, Ringheim A, Wall A, Forsberg A *et al.* Unidirectional Influx and Net Accumulation of PIB. *Open Neuroimag. J.* 2008; 2**:** 114-25.

4. Forsberg A, Engler H, Blomquist G, Langstrom B, Nordberg A. The use of PIB-PET as a dual pathological and functional biomarker in AD. *Biochim. Biophys. Acta* 2012; 1822(3)**:** 380-5.

5. Rostomian AH, Madison C, Rabinovici GD, Jagust WJ. Early 11C-PIB frames and 18F-FDG PET measures are comparable: a study validated in a cohort of AD and FTLD patients. *J. Nucl. Med.* 2011; 52(2)**:** 173-9.

6. Meyer PT, Hellwig S, Amtage F, Rottenburger C, Sahm U, Reuland P *et al.* Dual-biomarker imaging of regional cerebral amyloid load and neuronal activity in dementia with PET and 11C-labeled Pittsburgh compound B. *J. Nucl. Med.* 2011; 52(3)**:** 393-400.

7. Fu L, Liu L, Zhang J, Xu B, Fan Y, Tian J. Comparison of dual-biomarker PIB-PET and dual-tracer PET in AD diagnosis. *Eur Radiol* 2014; 24(11)**:** 2800-9.

8. Farid K, Hong YT, Aigbirhio FL, Fryer TD, Menon DK, Warburton EA *et al.* Early-phase $^{11}$C-PiB PET in amyloid angiopathy-related symptomatic cerebral hemorrage: potential diagnostic value?. *PLoS One* 2015; 10(10)**:** e0139926.

9. Paulson OB, Hasselbalch SG, Rostrup E, Knudsen GM, Pelligrino D. Cerebral blood flow response to functional activation. *J. Cereb. Blood Flow Metab.* 2010; 30(1)**:** 2-14.

10. Lammertsma AA, Hume SP. Simplified reference tissue model for PET receptor studies. *Neuroimage* 1996; 4(3 Pt 1)**:** 153-8.

11. Hsiao IT, Huang CC, Hsieh CJ, Hsu WC, Wey SP, Yen TC *et al.* Correlation of early-phase 18F-florbetapir (AV-45/Amyvid) PET images to FDG images: preliminary studies. *Eur. J. Nucl. Med. Mol. Imaging* 2012; 39(4)**:** 613-20.

12. Chiotis K, Saint-Aubert L, Savitcheva I, Jelic V, Anderson P, Jonasson M *et al.* Imaging in vivo tau pathology in Alzheimer's disease with THK5317 PET in a multimodal paradigm. *Eur. J. Nucl. Med. Mol. Imaging* (submitted).

13. McKhann GM, Knopman DS, Chertkow H, Hyman BT, Jack CR, Jr., Kawas CH *et al.* The diagnosis of dementia due to Alzheimer's disease: recommendations from the National Institute on Aging-Alzheimer's Association workgroups on diagnostic guidelines for Alzheimer's disease. *Alzheimer's & dementia : the journal of the Alzheimer's Association* 2011; 7(3)**:** 263-9.

14. Winblad B, Palmer K, Kivipelto M, Jelic V, Fratiglioni L, Wahlund LO *et al.* Mild cognitive impairment--beyond controversies, towards a consensus: report of the

International Working Group on Mild Cognitive Impairment. *J. Intern. Med.* 2004; 256(3)**:** 240-6.

15. Petersen RC, Smith GE, Waring SC, Ivnik RJ, Tangalos EG, Kokmen E. Mild cognitive impairment: clinical characterization and outcome. *Arch. Neurol.* 1999; 56(3)**:** 303-8.

16. Dubois B, Feldman HH, Jacova C, Dekosky ST, Barberger-Gateau P, Cummings J *et al.* Research criteria for the diagnosis of Alzheimer's disease: revising the NINCDS-ADRDA criteria. *Lancet Neurol.* 2007; 6(8)**:** 734-46.

17. Klunk WE, Engler H, Nordberg A, Wang Y, Blomqvist G, Holt DP *et al.* Imaging brain amyloid in Alzheimer's disease with Pittsburgh Compound-B. *Ann. Neurol.* 2004; 55(3)**:** 306-19.

18. Jonasson M, Wall A, Chiotis K, Saint-Aubert L, Wilking H, Sprycha M, Borg B, Thibblin A, Eriksson JP, Sörensen J, Antoni G, Nordberg A, Lubberink M. Tracer kinetic analysis of (S)-$^{18}$F-THK5117 as a PET tracer for assessing tau pathology. *J Nucl Med.* 2015 (in press).

19. Tago T, Furumoto S, Okamura N, Harada R, Adachi H, Ishikawa Y *et al.* Preclinical Evaluation of [F]THK-5105 Enantiomers: Effects of Chirality on Its Effectiveness as a Tau Imaging Radiotracer. *Mol. Imaging Biol.* 2015.

20. Harada R, Okamura N, Furumoto S, Furukawa K, Ishiki A, Tomita N et al. [(18)F]THK-5117 PET for assessing neurofibrillary pathology in Alzheimer's disease. Eur. J. Nucl. Med. Mol. Imaging 2015; 42(7): 1052-61.

21. Hammers A, Allom R, Koepp MJ, Free SL, Myers R, Lemieux L *et al.* Three-dimensional maximum probability atlas of the human brain, with particular reference to the temporal lobe. *Hum. Brain Mapp.* 2003; 19(4)**:** 224-47.

22. Nordberg A, Carter SF, Rinne J, Drzezga A, Brooks DJ, Vandenberghe R *et al.* A European multicentre PET study of fibrillar amyloid in Alzheimer's disease. *Eur. J. Nucl. Med. Mol. Imaging* 2013; 40(1)**:** 104-14.

23. Casanova R. Biological Parametric Mapping: A Statistical Toolbox for MultiModality Brain Image Analysis. *Neuroimage* 2007.

24. Robin X, Turck N, Hainard A, Tiberti N, Lisacek F, Sanchez JC *et al.* pROC: an open-source package for R and S+ to analyze and compare ROC curves. *BMC Bioinformatics* 2011; 12**:** 77.

25. Diedenhofen B, Musch J. cocor: a comprehensive solution for the statistical comparison of correlations. *PLoS One* 2015; 10(3)**:** e0121945.

26. de Leon MJ, Ferris SH, George AE, Reisberg B, Christman DR, Kricheff, II *et al.* Computed tomography and positron emission transaxial tomography evaluations of normal aging and Alzheimer's disease. *J. Cereb. Blood Flow Metab.* 1983; 3(3)**:** 391-4.

27. Friedland RP, Brun A, Budinger TF. Pathological and positron emission tomographic correlations in Alzheimer's disease. *Lancet* 1985; 1(8422)**:** 228.

28. Claus JJ, van Harskamp F, Breteler MM, Krenning EP, de Koning I, van der Cammen TJ *et al.* The diagnostic value of SPECT with Tc 99m HMPAO in Alzheimer's disease: a population-based study. *Neurology* 1994; 44(3 Pt 1)**:** 454-61.

29. Alsop DC, Dai W, Grossman M, Detre JA. Arterial spin labeling blood flow MRI: its role in the early characterization of Alzheimer's disease. *J. Alzheimers Dis.* 2010; 20(3)**:** 871-80.

30. Backman L, Andersson JL, Nyberg L, Winblad B, Nordberg A, Almkvist O. Brain regions associated with episodic retrieval in normal aging and Alzheimer's disease. *Neurology* 1999; 52(9)**:** 1861-70.

31. Yamaguchi H, Hirai S, Morimatsu M, Shoji M, Nakazato Y. Diffuse type of senile plaques in the cerebellum of Alzheimer-type dementia demonstrated by beta protein immunostain. *Acta Neuropathol.* 1989; 77(3)**:** 314-9.

32. Mirra SS, Gearing M, McKeel DW, Jr., Crain BJ, Hughes JP, van Belle G *et al.* Interlaboratory comparison of neuropathology assessments in Alzheimer's disease: a study of the Consortium to Establish a Registry for Alzheimer's Disease (CERAD). *J. Neuropathol. Exp. Neurol.* 1994; 53(3)**:** 303-15.

33. Minoshima S, Frey KA, Foster NL, Kuhl DE. Preserved pontine glucose metabolism in Alzheimer disease: a reference region for functional brain image (PET) analysis. *J. Comput. Assist. Tomogr.* 1995; 19(4)**:** 541-7.

34. Herholz K, Salmon E, Perani D, Baron JC, Holthoff V, Frolich L *et al.* Discrimination between Alzheimer dementia and controls by automated analysis of multicenter FDG PET. *Neuroimage* 2002; 17(1)**:** 302-16.

35. Talbot PR, Lloyd JJ, Snowden JS, Neary D, Testa HJ. Choice of reference region in the quantification of single-photon emission tomography in primary degenerative dementia. *Eur. J. Nucl. Med.* 1994; 21(6)**:** 503-8.

36. Pickut BA, Dierckx RA, Dobbeleir A, Audenaert K, Van Laere K, Vervaet A *et al.* Validation of the cerebellum as a reference region for SPECT quantification in patients suffering from dementia of the Alzheimer type. *Psychiatry Res.* 1999; 90(2)**:** 103-12.

37. Verfaillie SC, Adriaanse SM, Binnewijzend MA, Benedictus MR, Ossenkoppele R, Wattjes MP *et al.* Cerebral perfusion and glucose metabolism in Alzheimer's disease and frontotemporal dementia: two sides of the same coin? *Eur. Radiol.* 2015; 25(10)**:** 3050-9.

38. Huisman MC, van Golen LW, Hoetjes NJ, Greuter HN, Schober P, Ijzerman RG *et al.* Cerebral blood flow and glucose metabolism in healthy volunteers measured using a high-resolution PET scanner. *EJNMMI Res* 2012; 2(1)**:** 63.

39. Rodell AB, Aanerud J, Braendgaard H, Gjedde A. Washout allometric reference method (WARM) for parametric analysis of [$^{11}$C]PIB in human brains. *Front. Aging Neurosci.* 2013; 5(45)**:** 1-13.

40. Gjedde A, Aanerud J, Braendgaard H, Rodell AB. Blood-brain transfer of Pittsburgh compound B in humans. *Front. Aging Neurosci.* 2013; 5(70)**:** 1-9.

41. Smailagic N, Vacante M, Hyde C, Martin S, Ukoumunne O, Sachpekidis C. (1)(8)F-FDG PET for the early diagnosis of Alzheimer's disease dementia and other dementias

in people with mild cognitive impairment (MCI). *Cochrane Database Syst Rev* 2015; 1**:** CD010632.

## Figures

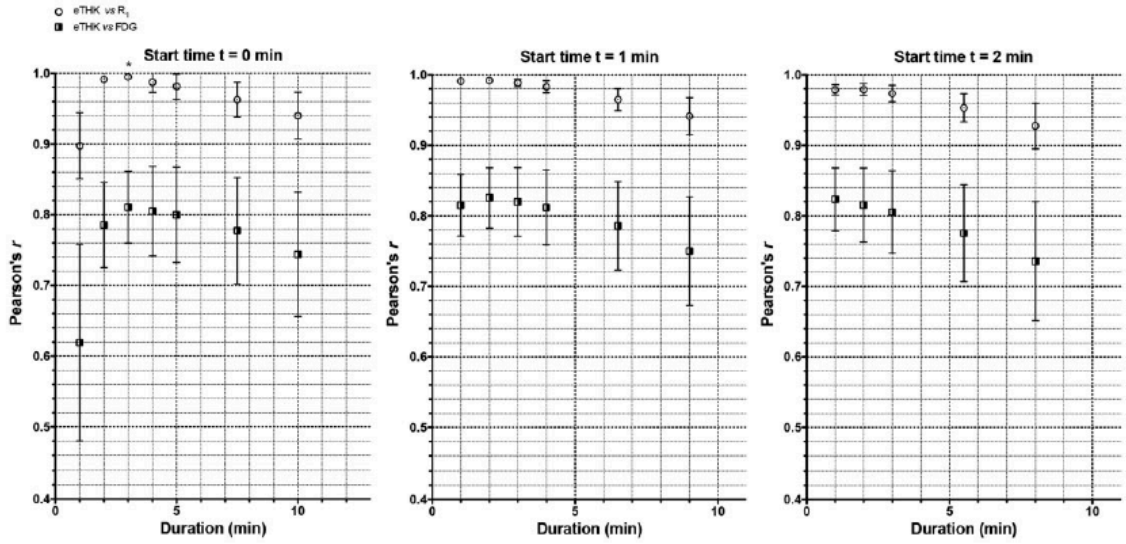


**Figure 1.** Optimization plots showing the correlation between early-phase [$^{18}$F]THK5317 (eTHK) and [$^{18}$F]THK5317 SRTM $R_1$ ($R_1$; open circles), and between eTHK and [$^{18}$F]FDG (FDG; half-filled squares), across different frame start times and durations. The ordinate shows correlation coefficients while the abscissa shows duration of data acquisition. The star label in the leftmost panel indicates the highest correlation achieved between eTHK and $R_1$.

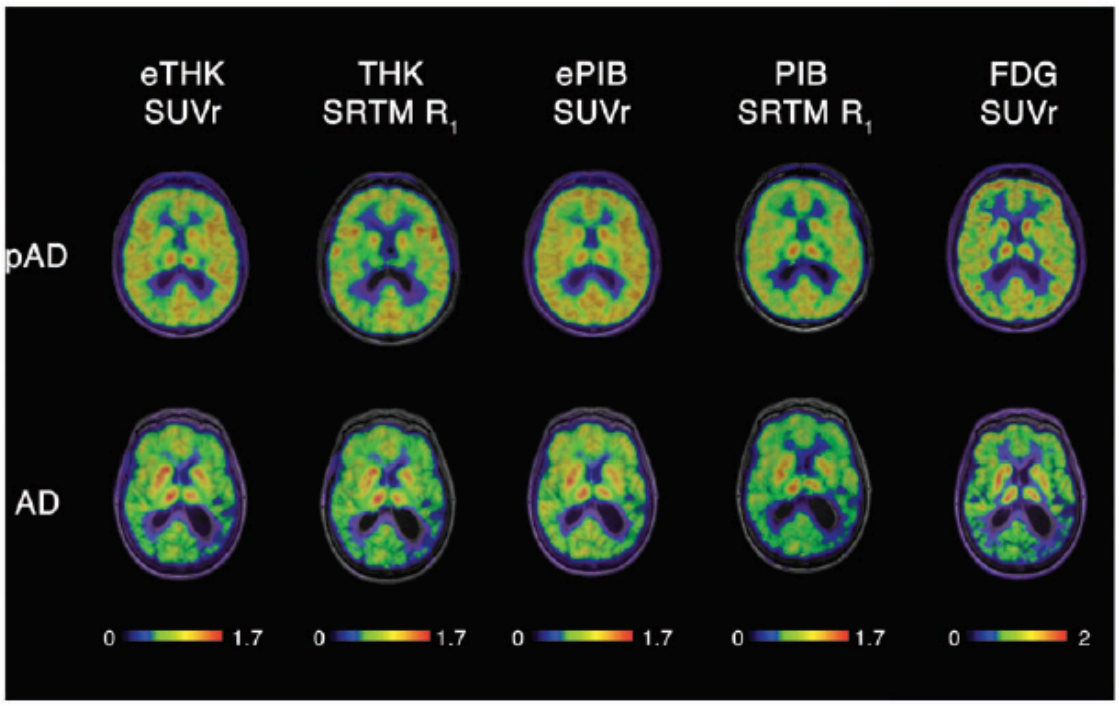


**Figure 2.** Axial views of representative [$^{18}$F]THK5317 early-phase SUVr and $R_1$ (eTHK SUVr and THK SRTM $R_1$, respectively), [$^{11}$C]PIB early-phase SUVr and $R_1$ (ePIB SUVr and PIB SRTM $R_1$, respectively) , and [$^{18}$F]FDG (FDG SUVr) PET images in a patient with prodromal AD (pAD, top row) and in a patient with AD dementia (bottom row).

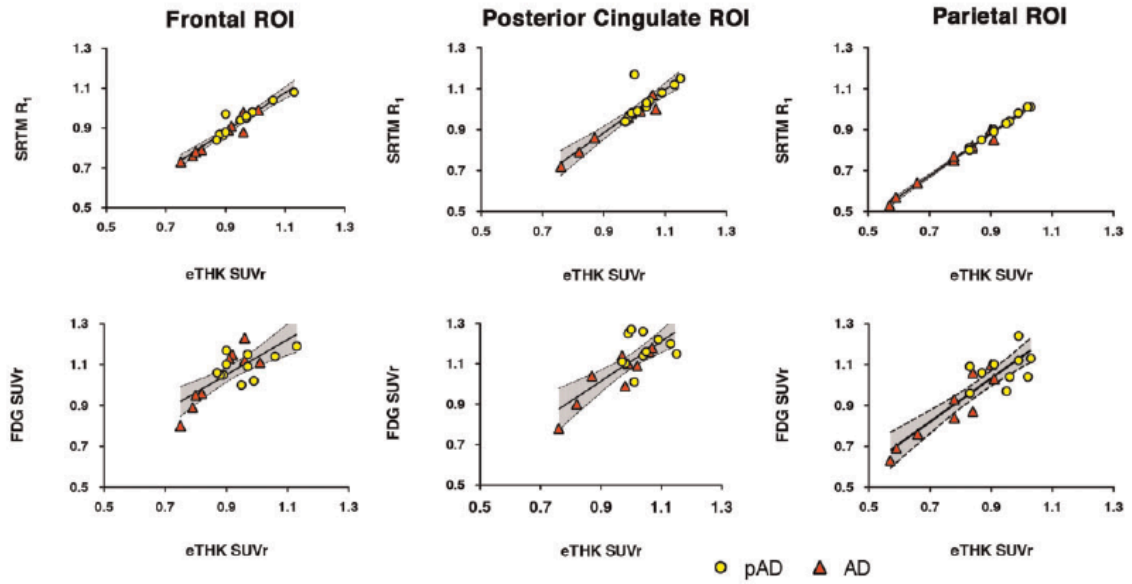


**Figure 3.** Linear regression scatter plots showing the relationship between early-phase [$^{18}$F]THK5317 SUVr (eTHK) and [$^{18}$F]THK5317 $R_1$ (top row) and between eTHK SUVr and [$^{18}$F]FDG SUVr and (bottom row), across frontal, posterior cingulate, and parietal ROIs. In addition to the best-fit linear regression line, shaded 95% confidence bands are shown.

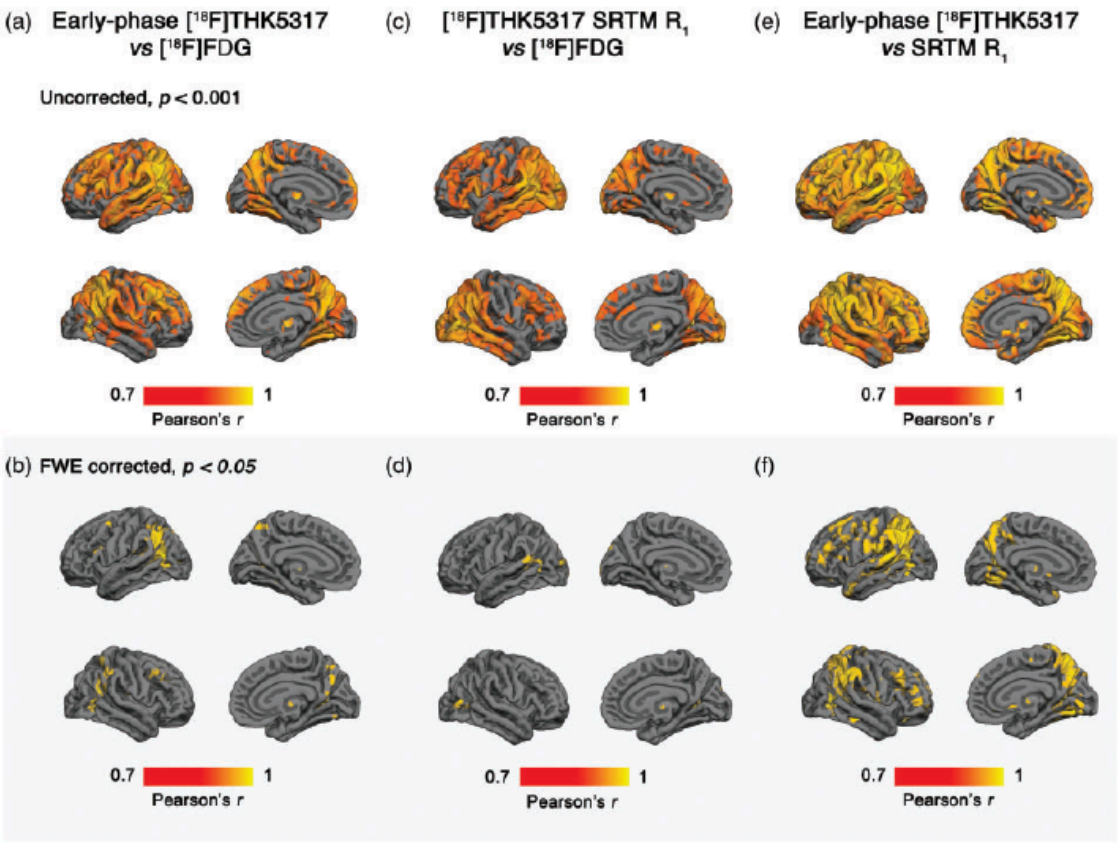


**Figure 4.** Biological Parametric Mapping derived voxelwise Pearson's correlation maps ($n$=20; top row, uncorrected with cluster extent $k \geq 20$ voxels, $p < 0.001$; bottom row, corrected for multiple comparisons using FWE, $p < 0.05$) showing (a, b) early-phase [$^{18}$F]THK5317 *vs* [$^{18}$F]FDG, (c, d) [$^{18}$F]THK5317 $R_1$ *vs* [$^{18}$F]FDG, and (e, f) early-phase [$^{18}$F]THK5317 *vs* [$^{18}$F]THK5317 $R_1$.

## Tables

## Table 1

ROI based Pearson's correlation coefficients for pairwise comparisons among [$^{18}$F]THK5317 ($R_1$, optimised early SUVr), [$^{11}$C]PIB ($R_1$, optimised early SUVr), and [$^{18}$F]FDG

| ROI | eTHK *vs* FDG SUVr | THK $R_1$ *vs* FDG SUVr | eTHK *vs* ePIB SUVr | eTHK SUVr *vs* THK $R_1$ | THK $R_1$ *vs* PIB $R_1$ |
|---|---|---|---|---|---|
| Frontal lobe | 0.747 (<0.001)* | 0.767 (<0.001)* | 0.807 (<0.001)* | 0.961 (<0.001)* | 0.860 (<0.001)* |
| Medial temporal lobe | 0.687 (<0.001)* | 0.801 (<0.001)* | 0.782 (<0.001)* | 0.934 (<0.001)* | 0.938 (<0.001)* |
| Lateral temporal lobe | 0.863 (<0.001)* | 0.858 (<0.001)* | 0.788 (<0.001)* | 0.991 (<0.001)* | 0.945 (<0.001)* |
| Posterior cingulate | 0.827 (<0.001)* | 0.831 (<0.001)* | 0.877 (<0.001)* | 0.990 (<0.001)* | 0.871 (<0.001)* |
| Occipital cortex | 0.911 (<0.001)* | 0.898 (<0.001)* | 0.930 (<0.001)* | 0.983 (<0.001)* | 0.911 (<0.001)* |
| Parietal cortex | 0.897 (<0.001)* | 0.896 (<0.001)* | 0.899 (<0.001)* | 0.958 (<0.001)* | 0.939 (<0.001)* |
| Global | 0.859 (<0.001)* | 0.863 (<0.001)* | 0.924 (<0.001)* | 0.983 (<0.001)* | 0.903 (<0.001)* |

Data in parentheses are *p* values. *Statistically significant correlations, FWE Bonferroni adjusted.

**Abbreviations:** Global, global cortical composite.

**Table 2**

Discriminative ability of [$^{18}$F]THK5317 (early-phase SUVr, $R_1$), [$^{11}$C]PIB (early-phase SUVr, $R_1$), and [$^{18}$F]FDG PET

| ROI | eTHK SUVr | THK $R_1$ | ePIB SUVr | PIB $R_1$ | FDG SUVr |
|---|---|---|---|---|---|
| Frontal lobe | 0.707 [0.458-0.955] | 0.687 [0.434-0.939] | 0.631 [0.367-0.894] | 0.621 [0.340-0.903] | 0.409 [0.119-0.696] |
| Medial temporal lobe | 0.702 [0.459-0.944] | 0.692 [0.443-0.940] | 0.645 [0.392-0.897] | 0.692 [0.451-0.933] | 0.667 [0.418-0.914] |
| Lateral temporal lobe | 0.833 [0.653-1.00] | 0.843 [0.666-1.00] | 0.600 [0.331-0.868] | 0.798 [0.599-1.000] | 0.773 [0.547-0.997] |
| Posterior cingulate | 0.742 [0.510-0.974] | 0.803 [0.607-0.998] | 0.700 [0.440-0.959] | 0.823 [0.611-1.000] | 0.813 [0.622-1.00] |
| Occipital cortex | 0.687 [0.420-0.953] | 0.742 [0.499-0.985] | 0.605 [0.331-0.879] | 0.641 [0.362-0.921] | 0.737 [0.492-0.983] |
| Parietal cortex | 0.889 [0.748-1.00] | 0.894 [0.745-1.00] | 0.655 [0.394-0.915] | 0.793 [0.578-1.000] | 0.864 [0.693-1.00] |
| Global | 0.818 [0.623-1.000] | 0.843 [0.671-1.000] | 0.778 [0.568-0.987] | 0.793 [0.594-0.992] | 0.810 [0.639-1.000] |

Results are presented as ROC AUC values [95% confidence intervals].

**Abbreviations:** Global, global cortical composite.

**Table 3**

Comparison of ROI based Pearson's correlation coefficients for [$^{18}$F]THK5317 (early-phase SUVr, $R_1$)/ [$^{11}$C]PIB (early-phase SUVr, $R_1$) vs [$^{18}$F]FDG PET.

| ROI | eTHK *vs* FDG SUVr | THK $R_1$ *vs* FDG SUVr | ePIB *vs* FDG SUVr | PIB $R_1$ *vs* FDG SUVr |
|---|---|---|---|---|
| Frontal lobe | 0.747 (<0.001)* | 0.767 (<0.01)* | 0.643 (<0.001)* | 0.776 (<0.001)* |
| Medial temporal lobe | 0.687 (<0.001)* | 0.801 (<0.001)* | 0.853 (<0.001)* | 0.856 (<0.001)* |
| Lateral temporal lobe | 0.863 (<0.001)* | 0.858 (<0.001)* | 0.791 (<0.001)* | 0.861 (<0.001)* |
| Posterior cingulate | 0.827 (<0.001)* | 0.831 (<0.001)* | 0.778 (<0.001)* | 0.820 (<0.001)* |
| Occipital cortex | 0.911 (<0.001)* | 0.898 (<0.001)* | 0.953 (<0.001)* | 0.963 (<0.001)* |
| Parietal cortex | 0.897 (<0.001)* | 0.896 (<0.001)* | 0.883 (<0.001)* | 0.924 (<0.001)* |
| Global | 0.859 (<0.001)* | 0.863 (<0.001)* | 0.884 (<0.001)* | 0.895 (<0.001)* |

Data in parentheses are p values. * Statistically significant correlations, FWE Bonferroni adjusted.

**Abbreviations:** Global, global cortical composite.

## Supplementary Table 1

Demographic and clinical characteristics according to diagnostic group

| Diagnosis | Age (y) | Sex (M: F) | MMSE score | ApoE ε4 positive, n (%) | [$^{11}$C]PIB PET positive, n (%) |
|---|---|---|---|---|---|
| Prodromal AD (*n*=11) | 73 (74, 65) | 5: 6 | 28 (29, 27.5) | 6 (55%) | 11 (100%) |
| AD dementia (*n*=9) | 67 (74, 60) | 2: 7 | 23 (25, 23) | 7 (78%) | 9 (100%) |

Values are reported as median (quartile3, quartile 1), or as n (%).

**Supplementary Table 2**

Cluster size and peak correlation coefficients for early-phase [$^{18}$F]THK5317 vs [$^{18}$F]FDG SUVr

| Brain region | L Activated Voxels | L Peak C | L % ROI Activation | R Activated Voxels | R Peak C | R % ROI Activation |
|---|---|---|---|---|---|---|
| Anterior superior temporal gyrus | 316 | 0.86 | 66.81 | 279 | 0.85 | 56.82 |
| Fusiform gyrus | 114 | 0.85 | 21.11 | 96 | 0.89 | 17.71 |
| Hippocampus | 67 | 0.87 | 23.18 | 35 | 0.80 | 14.18 |
| Lateral anterior temporal lobe | 205 | 0.89 | 65.08 | 142 | 0.82 | 40.23 |
| Lingual gyrus | 1124 **(38)** | 0.93 **(0.93)** | 69.99 **(2.37)** | 1268 **(179)** | 0.97 **(0.97)** | 73.72 **(10.41)** |
| Medial anterior temporal lobe | 106 | 0.83 | 15.84 | 101 | 0.79 | 14.33 |
| Middle and inferior temporal gyri | 988 **(157)** | 0.92 **(0.92)** | 55.26 **(8.78)** | 652 | 0.88 | 34.90 |
| Parahippocampal/ambient gyri | 78 | 0.84 | 18.80 | 55 | 0.83 | 14.44 |
| Posterior superior temporal gyrus | 1301 | 0.91 | 89.54 | 1074 **(22)** | 0.92 **(0.92)** | 82.87 **(1.7)** |
| Posterior temporal lobe | 3689 **(958)** | 0.98 **(0.98)** | 81.94 **(21.28)** | 3880 **(375)** | 0.97 **(0.97)** | 81.98 **(7.92)** |
| Insular cortex | 406 | 0.86 | 39.30 | 272 | 0.90 | 26.41 |

*(Continued)*

**Supplementary Table 2**

Cluster size and peak correlation coefficients for early-phase [$^{18}$F]THK5317 vs [$^{18}$F]FDG SUVr *(Continued)*

| Brain region | L Activated Voxels | L Peak C | L % ROI Activation | R Activated Voxels | R Peak C | R % ROI Activation |
|---|---|---|---|---|---|---|
| Cuneus | 729 **(133)** | 0.95 **(0.95)** | 55.52 **(10.13)** | 875 **(45)** | 0.94 **(0.94)** | 69.83 **(3.59)** |
| Occipital lobe, lateral remainder | 3168 **(454)** | 0.97 **(0.97)** | 70.00 **(10.03)** | 2414 **(148)** | 0.95 **(0.95)** | 53.24 **(3.26)** |
| Parietal lobe, inferolateral remainder | 4006 **(1487)** | 0.96 **(0.96)** | 96.21 **(35.71)** | 3927 **(750)** | 0.96 **(0.96)** | 93.61 **(17.88)** |
| Superior parietal gyrus | 3969 **(795)** | 0.96 **(0.96)** | 97.23 **(19.48)** | 3981 **(572)** | 0.96 **(0.96)** | 96.93 **(13.93)** |
| Anterior cingulate | 77 | 0.86 | 8.19 | 79 | 0.87 | 9.07 |
| Anterior orbital gyrus | 91 | 0.87 | 17.91 | 50 | 0.77 | 10.22 |
| Inferior frontal gyrus | 1461 **(69)** | 0.93 **(0.93)** | 71.37 **(3.37)** | 1245 | 0.90 | 62.94 |
| Lateral orbital gyrus | 82 | 0.84 | 22.91 | 42 | 0.78 | 10.88 |
| Medial orbital gyrus | 53 | 0.82 | 11.86 | 29 | 0.81 | 6.46 |
| Middle frontal gyrus | 3730 **(180)** | 0.93 **(0.93)** | 83.02 **(4.01)** | 3362 **(347)** | 0.96 **(0.96)** | 74.18 **(7.66)** |
| Posterior cingulate | 624 | 0.89 | 76.57 | 472 | 0.89 | 56.46 |
| Posterior orbital gyrus | 88 | 0.81 | 19.01 | 22 | 0.79 | 4.56 *(Continued)* |

## Supplementary Table 2

Cluster size and peak correlation coefficients for early-phase [$^{18}$F]THK5317 vs [$^{18}$F]FDG SUVr *(Continued)*

| Brain region | L Activated Voxels | L Peak C | L % ROI Activation | R Activated Voxels | R Peak C | R % ROI Activation |
|---|---|---|---|---|---|---|
| Pre-subgenual frontal cortex | 41 | 0.77 | 38.32 | - | - | - |
| Subgenual frontal cortex | 28 | 0.77 | 35.90 | - | - | - |
| Superior frontal gyrus | 2789 | 0.90 | 67.51 | 2842 **(77)** | 0.93 **(0.93)** | 65.18 **(1.77)** |
| Caudate nucleus | 131 **(36)** | 0.93 **(0.93)** | 75.29 **(20.69)** | 146 **(38)** | 0.93 **(0.93)** | 73.37 **(19.10)** |
| Thalamus | 131 | 0.93 | 75.29 | 146 | 0.93 | 73.37 |
| Precentral gyrus | 1848 | 0.91 | 68.50 | 1083 | 0.91 | 44.46 |
| Postcentral gyrus | 1820 | 0.91 | 78.75 | 1289 | 0.91 | 71.85 |

**Abbreviations:** L, left hemisphere; R, right hemisphere; C, Pearson correlation coefficient; -, cluster size was below the 20 voxel threshold.

Voxel-by-voxel positive correlations (uncorrected) between early-phase [$^{18}$F]THK5317 and [$^{18}$F]FDG PET, measured across all subjects pooled (n=20). Brain regions are from the 83-region Hammers atlas. For each cluster, the number of voxels and the maximum C value are reported. FWE corrected results are reported in brackets, bold type.

**Supplementary Table 3**

Cluster size and peak correlation coefficients for [$^{18}$F]THK5317 SRTM $R_1$ vs [$^{18}$F]FDG SUVr

| Brain region | L Activated Voxels | L Peak C | L % ROI Activation | R Activated Voxels | R Peak C | R % ROI Activation |
|---|---|---|---|---|---|---|
| Anterior superior temporal gyrus | 128 | 0.83 | 27.06 | 112 | 0.85 | 22.81 |
| Fusiform gyrus | 195 | 0.78 | 36.11 | 26 | 0.74 | 4.80 |
| Lateral anterior temporal lobe | 218 | 0.80 | 69.21 | 115 | 0.80 | 35.58 |
| Lingual gyrus | 1128 | 0.93 | 70.24 | 1098 **(55)** | 0.96 **(0.96)** | 63.84 **(3.20)** |
| Medial anterior temporal lobe | 38 | 0.77 | 5.68 | 100 | 0.82 | 14.18 |
| Middle and inferior temporal gyrus | 1652 | 0.90 | 92.39 | 1323 | 0.90 | 70.82 |
| Parahippocampus/ambient gyrus | 26 | 0.73 | 6.27 | - | - | - |
| Posterior superior temporal gyrus | 847 | 0.87 | 58.29 | 598 | 0.85 | 46.14 |
| Posterior temporal lobe | 3432 **(319)** | 0.97 **(0.97)** | 76.23 **(7.09)** | 3666 **(235)** | 0.96 **(0.96)** | 77.46 **(4.97)** |
| Brainstem | 27 | 0.79 | 9.78 | - | - | - |
| Insula | 257 | 0.86 | 24.88 | 137 | 0.82 | 13.30 |

*(Continued)*

**Supplementary Table 3**

Cluster size and peak correlation coefficients for [$^{18}$F]THK5317 SRTM $R_1$ vs [$^{18}$F]FDG SUVr *(Continued)*

| Brain region | L Activated Voxels | L Peak C | L % ROI Activation | R Activated Voxels | R Peak C | R % ROI Activation |
|---|---|---|---|---|---|---|
| Cuneus | 1107 **(54)** | 0.93 **(0.93)** | 84.31 **(4.11)** | 1012 **(45)** | 0.96 **(0.96)** | 80.77 **(3.59)** |
| Occipital lobe, lateral remainder | 4334 **(229)** | 0.95 **(0.95)** | 95.76 **(5.06)** | 4319 **(263)** | 0.95 **(0.95)** | 95.26 **(5.80)** |
| Parietal lobe, inferolateral remainder | 3159 **(208)** | 0.94 **(0.94)** | 75.86 **(5.00)** | 3116 **(71)** | 0.92 **(0.92)** | 74.28 **(1.69)** |
| Superior parietal gyrus | 3316 **(35)** | 0.92 **(0.92)** | 81.23 **(0.86)** | 2947 | 0.94 | 71.76 |
| Anterior cingulate | 192 | 0.78 | 20.43 | 302 | 0.79 | 34.67 |
| Anterior orbital gyrus | 69 | 0.80 | 13.58 | - | - | - |
| Inferior frontal gyrus | 1572 | 0.91 | 76.80 | 999 | 0.85 | 50.51 |
| Lateral orbital gyrus | 220 | 0.86 | 61.45 | 53 | 0.82 | 13.73 |
| Medial orbital gyrus | 42 | 0.85 | 9.40 | 30 | 6.68 | 0.76 |
| Superior frontal gyrus | 1701 | 0.86 | 41.18 | 1739 | 0.84 | 39.89 |
| Middle frontal gyrus | 2954 | 0.92 | 65.75 | 2373 **(38)** | 0.92 **(0.92)** | 52.36 **(0.84)** |
| Posterior cingulate | 226 | 0.85 | 27.73 | 71 | 0.75 | 8.49 |

*(Continued)*

## Supplementary Table 3

Cluster size and peak correlation coefficients for [$^{18}$F]THK5317 SRTM $R_1$ vs [$^{18}$F]FDG SUVr *(Continued)*

| Brain region | L Activated Voxels | L Peak C | L % ROI Activation | R Activated Voxels | R Peak C | R % ROI Activation |
|---|---|---|---|---|---|---|
| Posterior orbital gyrus | 21 | 0.76 | 4.54 | - | - | - |
| Caudate nucleus | 121 | 0.90 | 69.54 | 149 | 0.88 | 74.87 |
| Thalamus | 164 | 0.92 | 72.25 | 163 | 0.91 | 79.90 |
| Precentral gyrus | 788 | 0.86 | 29.21 | 433 | 0.88 | 17.78 |
| Postcentral gyrus | 719 | 0.86 | 31.11 | 377 | 0.82 | 21.01 |

**Abbreviations:** L, left hemisphere; R, right hemisphere; C, Pearson correlation coefficient; -, cluster size was below the 20 voxel threshold.

Voxel-by-voxel positive correlations (uncorrected) between [$^{18}$F]THK5317 SRTM $R_1$ and [$^{18}$F]FDG PET, measured across all subjects pooled (n=20). Brain regions are from the 83-region Hammers atlas. For each cluster, the number of voxels and the maximum C value are reported. FWE corrected results are reported in brackets, bold type.

**Supplementary Table 4**

Cluster size and peak correlation coefficients for early-phase [$^{18}$F]THK5317 and [$^{18}$F]THK5317 $R_1$.

| Brain region | L Activated Voxels | L Peak C | L % ROI Activation | R Activated Voxels | R Peak C | R % ROI Activation |
|---|---|---|---|---|---|---|
| Amygdala | 207 | 0.91 | 100.00 | 189 | 0.89 | 100.00 |
| Anterior superior temporal gyrus | 385 **(55)** | 0.93 **(0.93)** | 81.40 **(11.63)** | 371 | 0.89 | 75.56 |
| Fusiform gyrus | 317 **(59)** | 0.95 **(0.95)** | 58.70 **(10.93)** | 255 | 0.92 | 47.05 |
| Hippocampus | 289 **(67)** | 0.93 (0.93) | 100.00 **(23.18)** | 284 **(20)** | 0.92 **(0.92)** | 97.93 **(6.90)** |
| Lateral anterior temporal lobe | 264 **(88)** | 0.94 **(0.94)** | 83.81 **(27.94)** | 272 | 0.87 | 77.05 |
| Lingual gyrus | 1285 **(542)** | 0.96 **(0.96)** | 80.01 **(33.75)** | 1618 **(787)** | 94.07 **(45.76)** | 0.98 **(0.98)** |
| Medial anterior temporal lobe | 484 **(44)** | 0.93 **(0.93)** | 72.35 **(6.58)** | 534 | 0.88 | 75.74 |
| Middle and inferior temporal gyrus | 1224 **(519)** | 0.95 **(0.95)** | 68.46 **(29.03)** | 1371 **(125)** | 0.94 **(0.94)** | 73.39 **(6.69)** |
| Parahippocampal/ambient gyri | 379 **(40)** | 0.94 **(0.94)** | 91.33 **(9.64)** | 258 | 0.88 | 67.72 |
| Posterior superior temporal gyrus | 1446 **(758)** | 0.95 **(0.95)** | 99.52 **(52.17)** | 1285 | 0.93 **(0.93)** | 99.15 **(21.37)** |
| Brainstem | 119 | 0.89 | 43.12 | - | - | - |
| Insula | 949 **(145)** | 0.93 **(0.93)** | 9.187 **(14.04)** | 926 **(98)** | 0.93 **(0.93)** | 89.90 **(9.51)** |

*(Continued)*

**Supplementary Table 4**

Cluster size and peak correlation coefficients for early-phase [$^{18}$F]THK5317 and [$^{18}$F]THK5317 $R_1$ *(Continued)*

| Brain region | L Activated Voxels | L Peak C | L % ROI Activation | R Activated Voxels | R Peak C | R % ROI Activation |
|---|---|---|---|---|---|---|
| Cuneus | 1004 **(296)** | 0.96 **(0.96)** | 76.47 **(22.54)** | 1164 **(480)** | 92.90 **(38.31)** | 0.98 **(0.98)** |
| Occipital lobe, lateral remainder | 4334 **(229)** | 0.95 **(0.95)** | 95.76 **(5.06)** | 4319 **(263)** | 0.95 **(0.95)** | 95.26 **(5.80)** |
| Parietal lobe, inferolateral remainder | 4164 **(2904)** | 0.96 **(0.96)** | 100.00 **(69.74)** | 4177 **(2556)** | 0.96 **(0.96)** | 99.57 **(60.93)** |
| Superior parietal gyrus | 4082 **(2568)** | 0.96 **(0.96)** | 100.00 **(62.91)** | 4096 **(2410)** | 0.96 **(0.96)** | 99.73 **(58.68)** |
| Anterior cingulate | 316 | 0.90 | 33.40 | 236 | 0.87 | 27.10 |
| Anterior orbital gyrus | 508 **(55)** | 0.91 **(0.91)** | 100.00 **(10.83)** | 489 **(102)** | 0.92 **(0.92)** | 100.00 **(20.86)** |
| Inferior frontal gyrus | 2009 **(471)** | 0.96 **(0.96)** | 98.14 **(23.01)** | 1974 **(155)** | 0.92 **(0.92)** | 99.80 **(7.84)** |
| Lateral orbital gyrus | 355 | 0.90 | 99.16 | 325 | 0.90 | 84.20 |
| Medial orbital gyrus | 228 | 0.88 | 51.01 | 361 | 80.40 | 0.96 |
| Middle frontal gyrus | 4284 **(1329)** | 0.94 **(0.94)** | 95.35 **(29.58)** | 4338 **(1019)** | 0.93 **(0.93)** | 95.72 **(22.48)** |
| Posterior cingulate | 807 **(80)** | 0.94 **(0.94)** | 99.02 **(9.82)** | 738 **(26)** | 0.90 **(0.90)** | 88.28 **(3.11)** |
| Posterior orbital gyrus | 450 **(22)** | 0.91 **(0.91)** | 97.19 **(4.75)** | 215 | 44.61 | 0.91 *(Continued)* |

## Supplementary Table 4

Cluster size and peak correlation coefficients for early-phase [$^{18}$F]THK5317 and [$^{18}$F]THK5317 *(Continued)*

| Brain region | L Activated Voxels | L Peak C | L % ROI Activation | R Activated Voxels | R Peak C | R % ROI Activation |
|---|---|---|---|---|---|---|
| Posterior temporal lobe | 4392 **(2152)** | 0.97 **(0.97)** | 97.56 **(47.80)** | 4694 **(1341)** | 0.98 **(0.98)** | 98.23 **(28.33)** |
| Pre-subgenual frontal cortex | 107 | 0.89 | 100.00 | 68 | 0.91 | 100.00 |
| Straight gyrus | 72 | 0.83 | 17.82 | 259 | 0.86 | 54.64 |
| Subcallosal area | - | - | - | 20 | 0.91 | 95.24 |
| Subgenual frontal cortex | 58 | 0.86 | 74.36 | 58 | 0.91 | 98.31 |
| Superior frontal gyrus | 3795 **(357)** | 0.94 **(0.94)** | 91.87 **(8.64)** | 4064 **(335)** | 0.93 **(0.93)** | 93.21 **(7.68)** |
| Caudate nucleus | 163 **(81)** | 0.95 **(0.95)** | 93.68 **(46.55)** | 182 **(67)** | 0.93 **(0.93)** | 91.46 **(33.67)** |
| Putamen | 163 | 0.86 | 78.37 | 134 | 0.85 | 68.37 |
| Thalamus | 134 | 0.93 | 59.03 | 143 **(29)** | 0.94 **(0.94)** | 70.10 **(14.22)** |
| Precentral gyrus | 2642 **(417)** | 0.94 **(0.94)** | 97.92 **(15.36)** | 2262 **(277)** | 0.94 **(0.94)** | 92.86 **(11.37)** |
| Postcentral gyrus | 2292 **(691)** | 0.95 **(0.95)** | 99.18 **(29.90)** | 1780 **(348)** | 0.94 **(0.94)** | 99.22 **(19.40)** |

**Abbreviations:** L, left hemisphere; R, right hemisphere; C, Pearson correlation coefficient; -, cluster size was below the 20 voxel threshold.

Voxel-by-voxel positive correlations (uncorrected) between early-phase [$^{18}$F]THK5317 and [$^{18}$F]THK5317 $R_1$, measured across all subjects pooled (n=20). Brain regions are from the 83-region Hammers atlas. For each cluster, the number of voxels and the maximum C value are reported. FWE corrected results are reported in brackets, bold type.